

Finding proto-clusters to trace galaxy evolution: I. The finder and its performance

Kai Wang,^{1,2}* † H.J. Mo,² Cheng Li,¹ and Yangyao Chen^{1,2}

¹Department of Astronomy, Tsinghua University, Beijing 100084, China

²Department of Astronomy, University of Massachusetts Amherst, MA 01003, USA

Last updated 2020 May 22; in original form 2018 September 5

ABSTRACT

We develop a method to identify proto-clusters based on dark matter halos represented by galaxy groups selected from surveys of galaxies at high redshift. We test the performance of this method on halos in N-body simulations, and find that it can correctly identify more than 85% of the true proto-clusters with $\geq 95\%$ purity and with mass estimates typically within 0.25 dex from their true values. We show how the information provided by the proto-clusters can be used to link galaxies in present-day clusters of galaxies with their high redshift progenitors. Our tests show that the proto-clusters identified by our method can recover reliably the progenitor stellar mass distribution of galaxies, thereby providing an avenue to investigate the formation and evolution of present-day galaxy clusters and their member galaxies.

Key words: methods: statistical - galaxies: evolution - galaxies: groups: general - dark matter - large-scale structure of Universe

1 INTRODUCTION

Large surveys of galaxies are now available to investigate the statistical properties of the galaxy population at different redshifts. These observations can be used to study the evolution of the galaxy population over the history of the Universe. However, since galaxies at different redshifts have no individual causal relations, one can only study the evolution in a statistical way, by comparing the distribution functions of galaxy properties, such as stellar mass, star formation rate and spatial clustering. In order to use the observational data to make accurate and unbiased inferences on the evolution, it is necessary to connect galaxy populations at different redshifts in a meaningful way.

In the literature, two approaches have been adopted to connect galaxies at different redshift. The first is based on abundance matching, which assumes that ranks of galaxies in stellar mass are preserved as galaxies evolve with redshift (e.g. van Dokkum et al. 2010; Behroozi et al. 2013; Torrey et al. 2015, 2017; Hill et al. 2017; Mendel et al. 2020). Since this method uses only stellar mass to establish the connection, it ignores information about the evolution carried by other properties, such as the stellar population and environment of galaxies (Clauwens et al. 2016). More recently, Kipper et al. (2021) proposed a model for the evolution of the stellar mass and star formation rate of galaxies, and constrained the model parameters using observational data. However, this method is model-dependent and may be inaccurate when the redshift range covered is large. In addition, since galaxy properties are known to depend on environment, such as their halos (e.g. Weinmann et al. 2006; Wang et al. 2018), ignoring the environmental difference of galaxies will mix different evolutionary tracks, making the results difficult to interpret.

In the current paradigm of structure formation, galaxies form and evolve in dark matter halos, which are the virialized parts of the cosmic structure formed hierarchically through gravitational instability. Thus, the properties of the host halos of galaxies can provide additional information about the evolutionary tracks of galaxies. The formation and evolution of the halo population can be well understood using the state-of-the-art N-body simulations, and the link of a halo to its progenitors is provided by its merging tree. Since the progenitors of a galaxy hosted by a halo at the present day must be the galaxies that have formed in the progenitor halos, a link between the galaxy and its progenitors can be made through the connection of the halo with its progenitors. The second approach to connect galaxies across different redshifts is, therefore, to identify the progenitors of the most massive cluster galaxies in the local Universe as the most massive galaxies in high- z halos that are expected to evolve to $z = 0$ halos of mass similar to that of the clusters in question (e.g. Lidman et al. 2012; Cooke et al. 2019; DeMaio et al. 2020; Lin et al. 2013). This method is valid only if mergers among the high- z halos are negligible in the subsequent evolution. To overcome this problem, Zhao et al. (2017) developed a hybrid method to link the brightest cluster galaxies at low z to the brightest galaxies in the high density regions at high z , with the size of each of the regions chosen large enough so that subsequent mergers among the regions are negligible. However, since these investigations only traced the evolution of the most massive cluster galaxies following the main branches of the halo merger trees, they ignored a large number of galaxies that will evolve into satellite galaxies in $z = 0$ clusters. Clearly, a more general method using the information provided by the whole halo merger tree is needed to connect all galaxies in present-day clusters to their high- z progenitors.

The main objective of this paper is to develop a method that can link cluster galaxies to their progenitors reliably. A key component in our method is to group galaxies at high- z into common halos and identify proto-clusters that will evolve into clusters of given mass at

* Contact e-mail: wkcosmology@gmail.com

† Present address: Department of Astronomy, University of Massachusetts Amherst, MA 01003, USA

Table 1. Number of halos in the N-body simulation.

$\log(M_h/[h^{-1}M_\odot])$	$z = 0$	$z = 1$	$z = 2$
[12.0, ∞]	397,850	329,127	172,112
[14.0, 14.2]	1,307	161	5
[14.2, 14.5]	787	54	0
[14.5, 15.0]	257	4	0

the present time. As shown in Wang et al. (2020), with the high- z surveys of galaxies available now and in the near future, one can identify reliably galaxy groups/clusters to represent dark matter halos over a large mass range. One focus of the present paper is to develop a method to identify proto-clusters from such surveys. A number of proto-cluster identification methods have been proposed in the literature (See Overzier 2016, for a review), using densities defined by normal galaxies (Chiang et al. 2013, 2014; Diener et al. 2013; Franck & McGaugh 2016; Toshikawa et al. 2016; Lovell et al. 2018), Ly- α emitters (Chiang et al. 2015), Ly- α absorption systems (Cai et al. 2016; Lee et al. 2016; Cai et al. 2017), and star formation rate (Martinache et al. 2018). All these methods have to be calibrated using semi-analytical models and/or hydrodynamic simulations to ensure that the identified systems represent proto-clusters with well-defined mass. In comparison, our method based on halos mitigates the uncertainties introduced by baryonic processes in galaxy formation, so that it can be tested and calibrated using cosmological N-body simulations.

The paper is organized as follows. The simulation data and the empirical model of galaxy formation used for our analyses are presented in § 2. Our proto-cluster finder and the test results of its performances are presented in § 3. We describe how to use the information provided by proto-clusters to link halos and galaxies at different redshifts in § 4. Finally, we summarize our main results in § 5.

2 SIMULATION DATA FOR TESTING

2.1 The simulation and the empirical model of halo occupation

We use the cosmological simulation, ELUCID (Wang et al. 2016), combined with an empirical model of galaxy formation to construct mock galaxy samples to test our method. ELUCID was run with L-GADGET, a memory-optimized version of GADGET-2 (Springel et al. 2005), using 3072^3 dark matter particles, each with a mass of $3.09 \times 10^8 h^{-1} M_\odot$, in a periodic box with a side length of $500h^{-1} \text{cMpc}$. The simulation uses cosmological parameters based on WMAP5 (Dunkley et al. 2009): $\Omega_m = 0.258$, $\Omega_\Lambda = 0.742$, $H = 100h \text{ km s}^{-1} \text{ Mpc}^{-1}$ with $h = 0.72$, and $\sigma_8 = 0.80$. The simulation covers the structure evolution from $z = 100$ to 0, and records 100 snapshots from $z = 19$ to 0. Dark matter halos and subhalos are identified using the friend-of-friend (FoF) and SUBFIND algorithms (Springel et al. 2001), and halo merger trees are constructed to trace the merging histories of individual halos using the code provided by Springel et al. (2005).

We populate dark matter halos in ELUCID with galaxies using the empirical model developed in Lu et al. (2014, 2015). This model treats central and satellite galaxies separately. For central galaxies, the star formation rate is parameterized as a function of redshift and host halo mass. For satellite galaxies, the star formation rate is assumed to decline with time until the satellite merges with the central galaxy. The free parameters are constrained with the observed galaxy stellar mass function spanning a large range of redshift and the cluster

galaxy luminosity function in the low- z Universe. The positions and velocities of individual galaxies are assigned according to those of halos (for central galaxies) and subhalos (for satellite galaxies). The details of the implementation of the empirical model to the simulation can be found in Chen et al. (2019).

2.2 Proto-clusters in the simulation

We use all dark matter halos with mass above $10^{12} h^{-1} M_\odot$ at a given redshift z to trace proto-clusters. This choice of mass threshold is motivated by the fact that such halos can be identified reliably as galaxy groups at different redshifts (Wang et al. 2020; Looser et al. 2021). In this paper, we use halos at $z = 0, 1$ and 2 (see Table 1). We define a proto-cluster as the set of dark matter halos at $z > 0$ that end up in a common descendant halo at $z = 0$. Thus, a proto-cluster is the collection of progenitor halos at $z > 0$ for a dark matter halo at $z = 0$. In the literature, investigations of proto-clusters have been focused on relatively massive systems which correspond to massive dark matter halos at $z = 0$, e.g. with halo mass $M_0 \gtrsim 10^{14} h^{-1} M_\odot$. Thus, some of the massive progenitors contained in a proto-cluster may themselves be high- z clusters according to our definition. For clarity, we use M_0 to denote the descendant halo mass at $z = 0$, and M_h to denote the progenitor dark matter halo mass (See Table 2). We retrieve all the progenitor halos with $M_h \geq 10^{12} h^{-1} M_\odot$ for each descendant halo with $M_0 \geq 10^{12} h^{-1} M_\odot$ following its merger tree in the simulation. We thus obtain a set of samples of present-day halos and their true proto-clusters at a given high redshift. These links between present-day halos and their proto-clusters will be used to calibrate and test our method to identify proto-clusters from observational data.

2.3 Redshift-space distortion

In real observations, we can only infer the position of a galaxy from (RA, Dec, z), where the first two specify the position of an object in the sky, while the redshift z can be converted to a line-of-sight distance. However, the distance obtained from z is contaminated by the peculiar velocity of the object owing to the redshift-space distortion. For our problem, this contamination can be divided into two categories: small-scale Finger-of-God effect caused by the virial motion of galaxies inside individual dark matter halos (see Jackson 1972), and large-scale Kaiser effect owing to the peculiar motion of dark matter halos produced by the gravitational interactions on super-halo scales (see Kaiser 1987). Since our method relies on halos to trace proto-clusters, and since the Finger-of-God effect is corrected in the halo/group finding process (Yang et al. 2005), we only need to consider the Kaiser effect.

To mimic the Kaiser effect in our analysis, we modify the positions of dark matter halos along one chosen direction, assumed to be the \hat{X} direction. For a dark matter halo at $\mathbf{r} = X\hat{X} + Y\hat{Y} + Z\hat{Z}$ with peculiar velocity \mathbf{v} in a box with redshift z , we update its \hat{X} -component by

$$X \leftarrow X - D_c(z) + D_c(z'), \quad z' \equiv (z+1) \left(\frac{\mathbf{v} \cdot \hat{X}}{c} + 1 \right) - 1 \quad (1)$$

where $D_c(z)$ is the comoving distance at redshift z , and c is the speed of light. Halos near the edge of the simulation box are properly taken care of by using the periodic boundary conditions.

2.4 Descendant halo mass calibration

Descendant halo mass plays a critical role in connecting galaxies at high- z to their low- z counterparts. In the literature the descendant

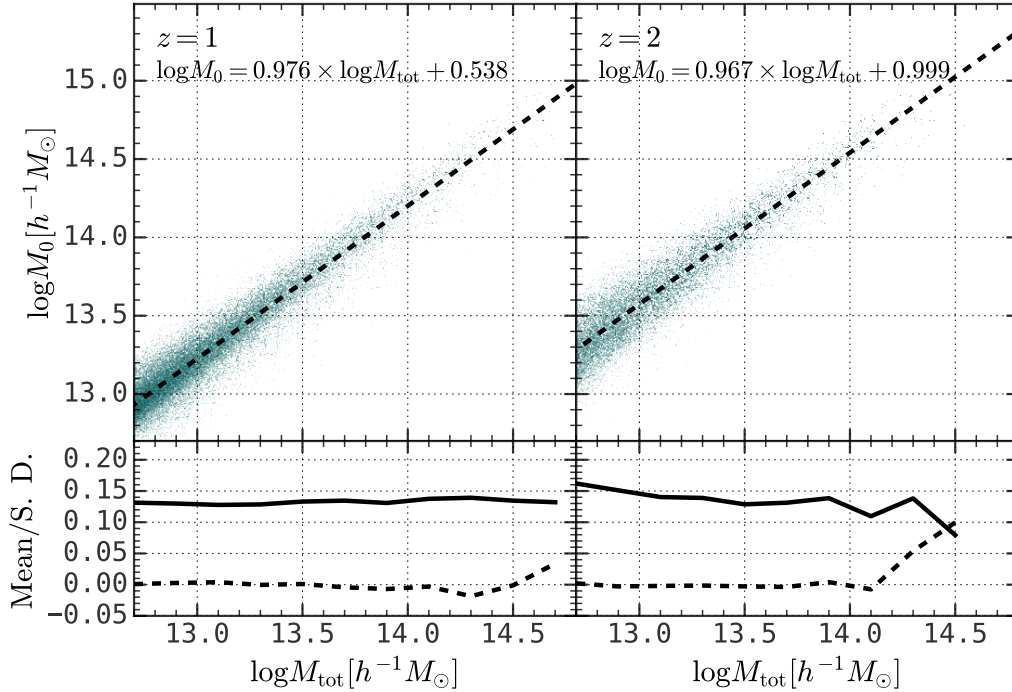


Figure 1. The *upper* panels show the relation between the total halo mass, M_{tot} , and the descendant halo mass, M_0 , and the lines are the fitting functions shown in the upper left corner. In the *lower* panels, the solid lines show the standard deviation from the fitting function, and the dashed lines show the mean of $\log(M_{0,\text{fitting}}/M_0)$, where $\log(M_{0,\text{fitting}})$ is the descendant mass obtained from the fitting function. The *left* panels are for $z = 1$, and the *right* panels for $z = 2$.

halo mass is usually estimated from the overdensity of a given class of tracers, such as galaxies, halos and dark matter (e.g. Chiang et al. 2013; Steidel et al. 1998, 2005). Here we choose to calibrate the descendant halo mass using the total halo mass, M_{tot} , which is the sum of the masses of all the halos in the proto-cluster with $M_h \geq 10^{12} h^{-1} M_\odot$. As shown in Fig. 1, there is a well-defined relation between M_{tot} and M_0 , which is well described by a linear function. The standard deviation of the relation is quite small, typically below 0.15 dex for the descendant mass $M_0 > 10^{13} h^{-1} M_\odot$. Thus, the masses of the proto-clusters can be estimated reliably using calibrations from N -body simulations. We will use such calibrations to estimate the descendant halo masses for candidate proto-clusters.

3 THE PROTO-CLUSTER FINDING ALGORITHM AND ITS PERFORMANCE

In this section, we present a proto-cluster finding algorithm based on the Friends-of-Friends (FoF) method, and test its performance. The FoF algorithm was used to identify dark matter halos in N -body simulations and to identify galaxy groups in galaxy surveys (Davis et al. 1985; Eke et al. 2004; Knobel et al. 2009; Wang et al. 2020). Our proto-cluster finding algorithm uses the distribution of dark matter halos in redshift space, where halos are assumed to be identified through a group finding process, such as those described in Yang et al. (2005, 2007) and Wang et al. (2020). This approach mitigates all the baryon-related physics in identifying virialized halos and is, therefore, applicable as long as a complete sample of relatively massive halos/groups (e.g. $M_h > 10^{12} h^{-1} M_\odot$) is available.

3.1 The proto-cluster finder

For a given dark matter halo distribution in the redshift space, we group the i -th and j -th halos together if they satisfy the following criteria:

$$l_{\parallel} \cdot R_{\text{vir}} \geq |X_i - X_j| \quad (2)$$

$$l_{\perp} \cdot R_{\text{vir}} \geq \sqrt{(Y_j - Y_k)^2 + (Z_j - Z_k)^2} \quad (3)$$

where l_{\parallel} and l_{\perp} are two free parameters, $R_{\text{vir}} = \max(R_{\text{vir},i}, R_{\text{vir},j})$, and the halo virial radii, $R_{\text{vir},i}$ and $R_{\text{vir},j}$, are calculated using the package Halotools (Hearin et al. 2017). Again, X is the distance along the line-of-sight, while Y and Z are in the perpendicular directions.

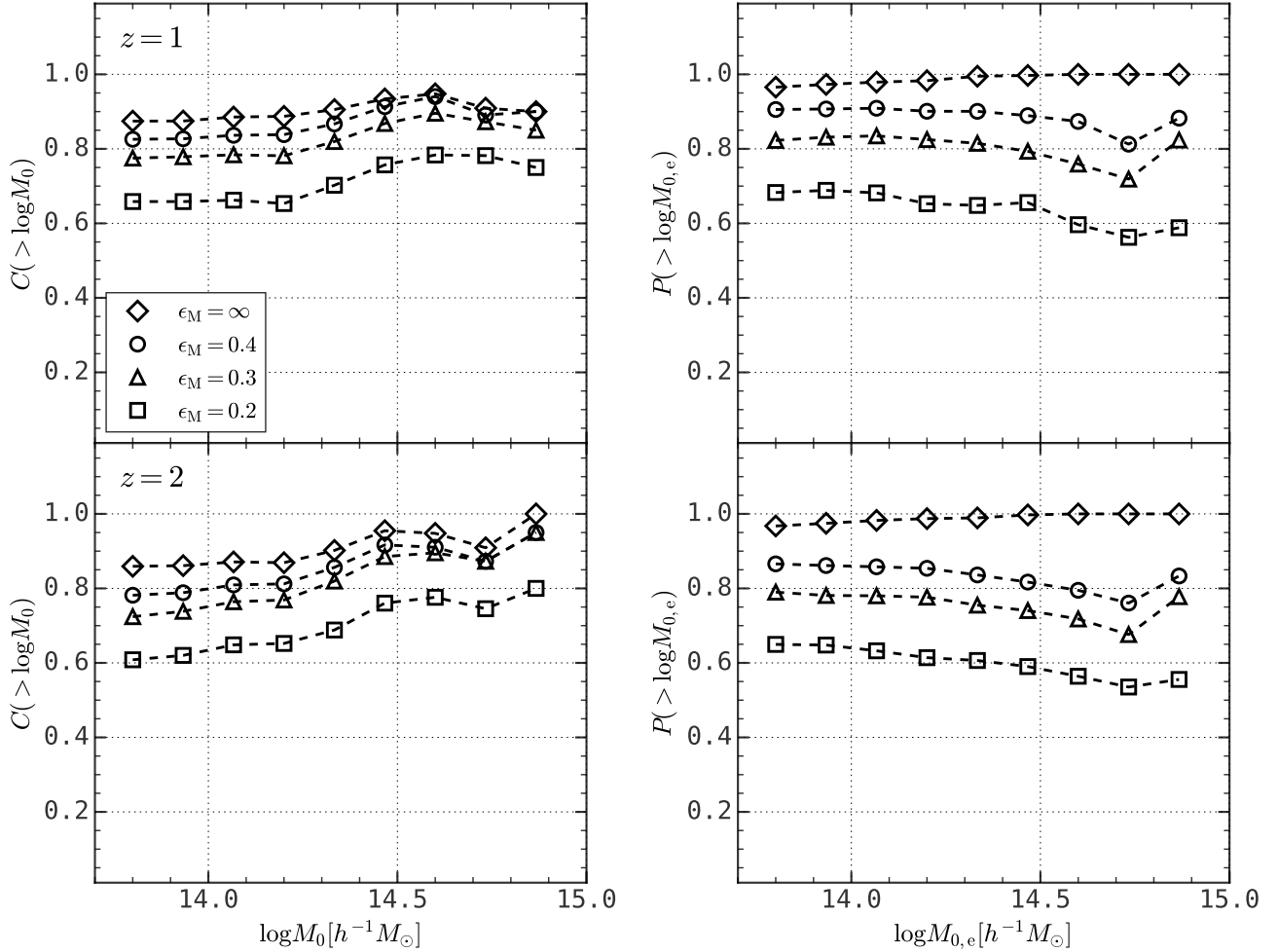
For all halos that are linked into a candidate proto-cluster according to the above criteria, we calculate a total mass, M_{tot} , which is the sum of the masses of all these halos. We then assign to each candidate proto-cluster a descendant halo mass, $M_{0,e}$, using the fitting function in Fig. 1.

3.2 Completeness and purity of the identified proto-cluster population

In this subsection, we quantify the performance of our proto-cluster finding algorithm in terms of the completeness and purity of the identified proto-cluster population. We define the completeness (C) as the fraction of correctly identified proto-clusters among the true population, and purity (P), as the fraction of the correctly identified proto-clusters among all the candidate proto-clusters. To do this, we need to define what we mean by a correct identification of a proto-cluster. We use the most massive halo (MMH) selected into

Table 2. Terminologies and symbols used in the paper.

Terminology	Explanation
true proto-cluster	the collection of the progenitor halos and galaxies for a dark matter halo at $z = 0$
candidate proto-cluster	the collection of halos identified by the proto-cluster finder
halo mass (M_h)	mass of a dark matter halo
descendant halo mass (M_0)	mass of the descendant dark matter halo at $z = 0$
estimated descendant halo mass ($M_{0,e}$)	estimated mass of the descendant dark matter halo at $z = 0$
stellar mass of galaxy (M_*)	stellar mass of a galaxy
stellar mass of descendant galaxy ($M_{*,0}$)	stellar mass of a descendant galaxy at $z = 0$

**Figure 2.** Completeness (*left*) and purity (*right*) of the proto-cluster identification at $z = 1$ (*upper*) and $z = 2$ (*lower*) as functions of descendant halo mass, M_0 , with different mass error tolerance (see text for detailed explanations).

a candidate proto-cluster to link it to a true proto-cluster. Thus, if the MMH of the true proto-cluster is the MMH of a candidate proto-cluster, we then say that the true proto-cluster is correctly identified. On the other hand, if the MMH of the candidate proto-cluster is the MMH of one true proto-cluster, the candidate proto-cluster is said to be a correct identification of a true proto-cluster. In addition,

when calculating C and P , we also include a quantity of mass error tolerance, so that the correct identification of a proto-cluster also requires that

$$|\log(M_0) - \log(M_{0,e})| < \epsilon_M \quad (4)$$

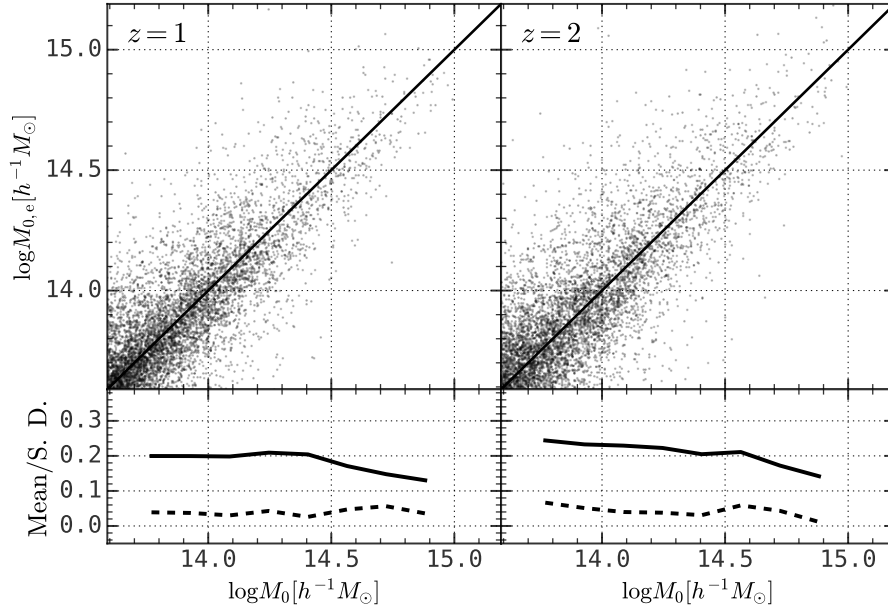


Figure 3. Comparison of the descendant halo mass between the true value and the estimated value at $z = 1$ (left) and $z = 2$ (right). The dashed lines in the upper panels are the one-to-one line. In the lower panels, the solid and dashed lines show the standard deviation and mean of $\log(M_0/M_{0,e})$, respectively.

where M_0 is the true descendant halo mass at $z = 0$, $M_{0,e}$ is the estimated descendant halo mass of the matched candidate proto-cluster, and ϵ_M is a factor characterizing the mass error tolerance.

In Fig. 2, we present the completeness (C) and purity (P) for proto-clusters identified at $z = 1$ and 2 as function of the true descendant halo mass. Results are shown for four different choices of the mass error tolerance: $\epsilon_M = 0.2, 0.3, 0.4$ and ∞ , with $\epsilon_M = \infty$ corresponding to no mass accuracy requirement. We see that, if no mass accuracy requirement is used, i.e. for $\epsilon_M = \infty$, more than 89% (87%) of the proto-clusters with descendant halo mass above $10^{14} h^{-1} M_{\odot}$ are identified at $z = 1$ ($z = 2$), with purity larger than as 98% (98%). For $\epsilon_M = 0.4$ dex, more than 84% (81%) of the proto-clusters with descendant halo mass above $10^{14} h^{-1} M_{\odot}$ are identified at $z = 1$ ($z = 2$), with purity larger than as 91% (86%). Both C and P decrease by about 20% when a more restrictive mass criterion, $\epsilon_M = 0.2$, is used.

3.3 Descendant halo mass

We apply the relations between M_{tot} and M_0 obtained in § 2.4 to estimate the descendant mass, $M_{0,e}$ for each identified proto-cluster using the total mass of its member halos selected by the proto-cluster finder. Fig. 3 shows the comparison between $M_{0,e}$ and the true descendant halo mass, M_0 . As one can see, most of the proto-clusters (black dot) lie close to the one-to-one line, with the standard deviation (shown by the black solid lines in lower panels) typically about 0.20 dex and 0.25 dex at $z = 1$ and $z = 2$, respectively. In real applications, there are also uncertainties in the masses assigned to dark matter halos. Wang et al. (2020) tested the halo mass estimate using realistic mock catalogs based on the PFS survey (Takada et al. 2014), and found that the typical error in the mass estimate is about 0.2 dex. Including this uncertainty in the estimate of M_{tot} increases the standard deviation of $M_{0,e}$ to 0.3 dex (See Fig. A2).

3.4 Completeness and purity of member halos

Another important performance measurement concerns the member halos identified, in terms of the fractions of the true member halos and the interlopers, in each candidate proto-cluster. This kind of performance has been used to test the galaxy group finder in Yang et al. (2007). Here we modify the definition slightly. We define the membership completeness, C_M , and membership purity, P_M , as

$$C_M \equiv N_{\text{ST}}/N_T \quad (5)$$

$$P_M \equiv N_{\text{ST}}/N_S \quad (6)$$

where N_S is the total number of halos selected into a candidate proto-cluster, N_T is the number of halos in the corresponding true proto-cluster, and N_{ST} is the number of true member halos in the candidate proto-cluster. Thus, $C_M = P_M = 1$ for a perfect membership assignments.

The member completeness and purity are shown in Fig. 4. At $z = 1$ ($z = 2$), $\sim 60\%$ ($\sim 80\%$) of the identified proto-clusters have completeness of $\geq 80\%$, while $\sim 56\%$ ($\sim 80\%$) of them have purity $\geq 80\%$. We note that, in terms of C_M and P_M , our proto-cluster finder performs equally well for different descendant halo mass bins. This suggests that we can use the same finder for proto-clusters of different descendant halo masses by re-scaling the selection rule with the descendant halo mass.

3.5 Conditional mass function of member halos

The conditional halo mass function is defined as

$$\Phi(M_h | M_0^l, M_0^u) \equiv \frac{dN(M_h | M_0 \in [M_0^l, M_0^u])}{N_{\text{PC}} d \log M_h} \quad (7)$$

where $N(M_h | M_0 \in [M_0^l, M_0^u])$ is the halo mass distribution of all the halos at redshift z whose descendant halo mass at $z = 0$ is in the range of $[M_0^l, M_0^u]$, and N_{PC} is the number of proto-clusters in that descendant halo mass range. So defined, the conditional halo

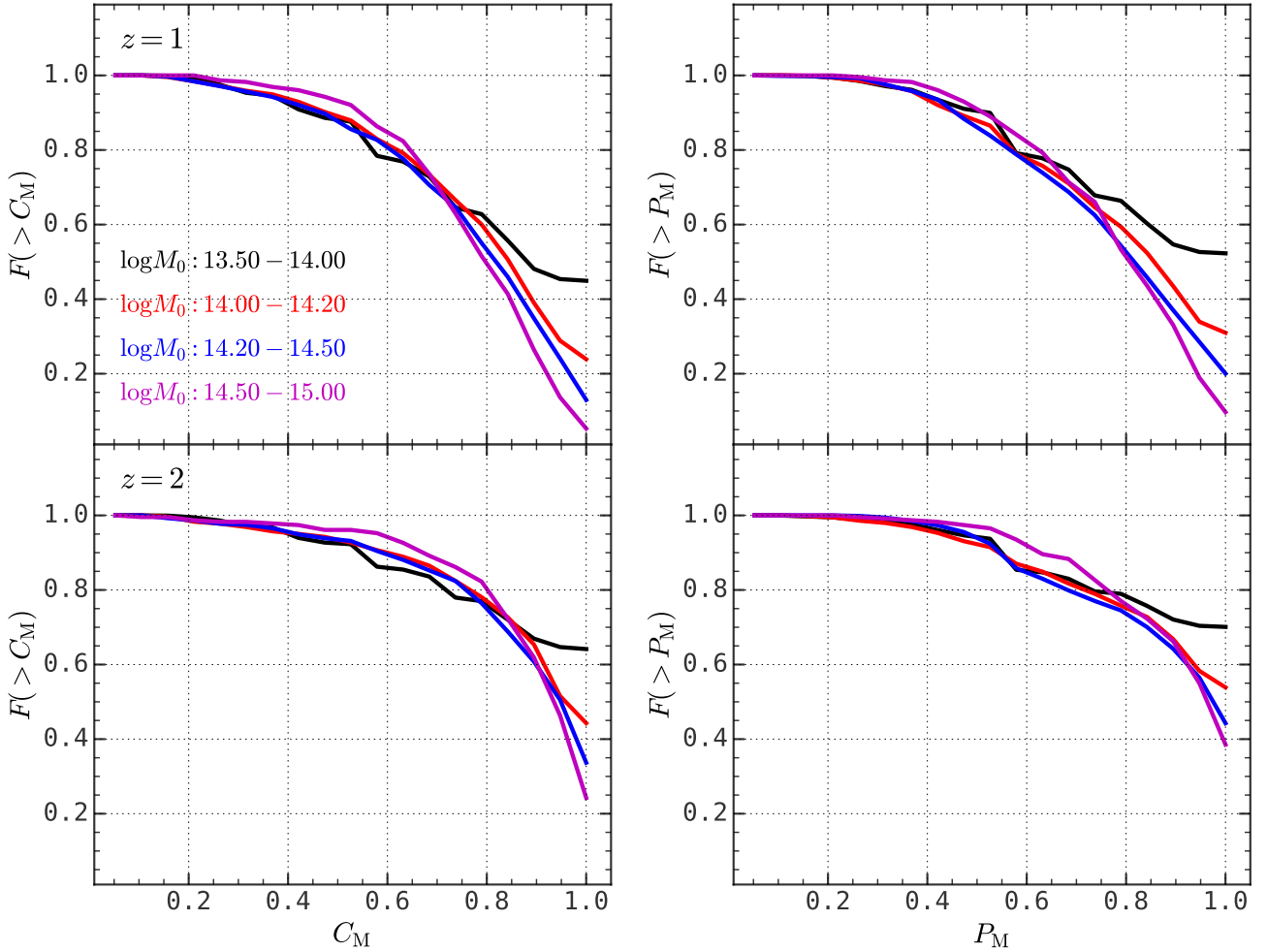


Figure 4. The accumulated membership completeness (*left*) and purity (*right*) for the proto-clusters identified and matched with true proto-clusters at $z = 1$ (*upper panels*) and $z = 2$ (*lower panels*).

mass function describes the average number of halos of a given mass that are contained in proto-clusters of a given M_0 . The results of the conditional halo mass function obtained from our identified proto-clusters are shown as circles in Fig. 5 (Mock-1), and are compared to those obtained from the true proto-clusters (the solid curves). For comparison, the dashed curves are for the most massive halos (MMH) in individual proto-clusters. The conditional halo mass functions above the halo mass limit of $10^{12} h^{-1} M_\odot$ are well reproduced for proto-clusters with $M_0 = 10^{14} h^{-1} M_\odot$ to $10^{15} h^{-1} M_\odot$ at both $z = 1$ and $z = 2$. Here we only present the result of one descendant halo mass bin for clarity, and we can reproduce the function in other bins equally well. Even if we include a dispersion of 0.20 dex in the estimates of M_h , as expected from the uncertainties produced by the group finder in real applications (Wang et al. 2020), the results do not change much (See appendix. A).

The good match between the recovered conditional halo mass function and the true one indicates that the member halos of proto-clusters are reliably identified by our method. Since these halos are the progenitors of sub-halos in present-day main halos with given M_0 , and since member galaxies in present-day galaxy clusters are expected to be connected with the sub-halos, the proto-clusters and

their member halos identified using our method can be used to link cluster galaxies with their high- z progenitors statistically.

4 LINKING HIGH REDSHIFT PROGENITORS TO LOCAL CLUSTERS

An important problem in astronomy is to understand how galaxies evolve with redshift. Various methods have been proposed to link galaxy populations at different redshifts statistically. For example, one can directly link local galaxies with their high- z progenitors or link high- z galaxies with their low- z descendants using a rank-order/abundance matching method (van Dokkum et al. 2010; Behroozi et al. 2013). One can also connect galaxies at different redshifts using stellar ages (Cimatti et al. 2012). Finally, one may also study the evolution of the brightest cluster galaxies by connecting dark matter halos at different redshifts (Lidman et al. 2012; Lin et al. 2013; Cooke et al. 2019; DeMaio et al. 2020). In this section, we show how we can use the information provided by proto-clusters to link halos and galaxies at high- z to their descendants at the present, and vice versa.

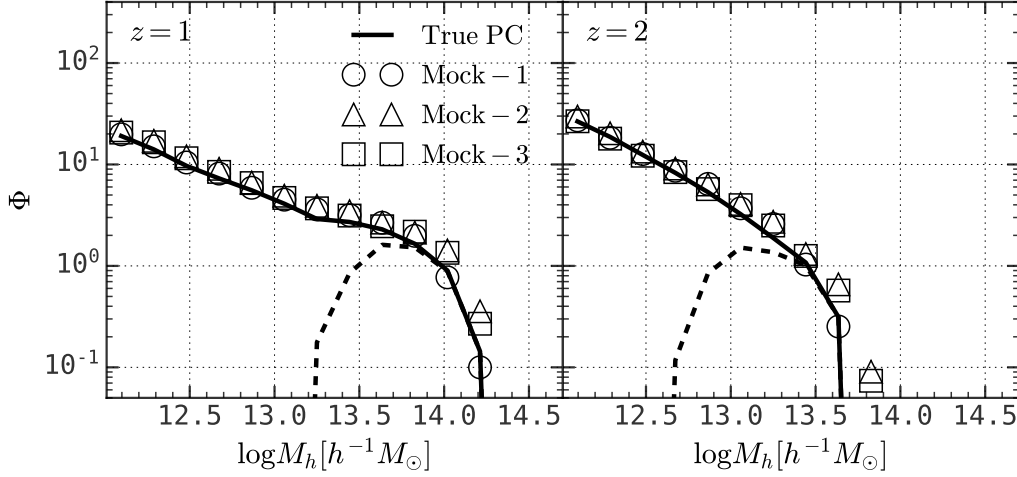


Figure 5. Conditional halo mass function at $z = 1$ (left) and $z = 2$ (right) for proto-clusters with $14.2 \leq \log M_{0,e} / [h^{-1} M_{\odot}] \leq 14.5$. The black solid lines are measured from the true proto-clusters, the dashed lines are the MMH component of the true conditional halo mass function, the circles are measured from the candidate proto-cluster catalog. The triangles and squares are results for Mock-2 and Mock-3 defined in Appendix A.

4.1 High redshift dark matter halos and their descendants

Let us first examine how halos selected at high z are linked to halos at $z = 0$. To do this, we select all halos of a given mass at a given high z and study the mass distribution of their descendants at $z = 0$. The blue histograms in Fig. 6 show the descendant mass (M_0) distribution for halos identified at $z = 1$ and $z = 2$, respectively. For a given halo mass bin, $M_1 \leq M_h \leq M_2$, the M_0 distribution is peaked at a value that is a couple of times larger than the average mass of the halos selected. Most of the low-mass halos will end up in relatively low-mass descendant halos at $z = 0$. However, there is an extended tail towards high M_0 , which is expected to be dominated by halos in massive proto-clusters. We can use the information provided by the identified proto-clusters to refine the connection between high- z halos and their $z = 0$ descendants. To this end, we split halos into several bins of the estimated descendant mass ($M_{0,e}$), and obtain the true descendant mass (M_0) distributions for halos in each $M_{0,e}$ bin. As an example, the black histograms in the figure show these distributions for $14.2 \leq \log M_{0,e} / [h^{-1} M_{\odot}] \leq 14.5$ (indicated by the vertical gray bands). Results for other bins are qualitatively the same and not shown here. One can see that the peak of the distribution is now roughly at the gray region, indicating that the use of the constraint on $M_{0,e}$ can effectively select the progenitors of the halos at $z = 0$. There is, however, a long tail at the low descendant mass end, which is contributed by interloper halos in the identified proto-clusters.¹ We can reduce the contribution of these interlopers by eliminating halos in the outskirts of the identified proto-clusters. To do this, we

first define two effective radii,

$$R_{e,\parallel} = \sqrt{\frac{\sum_i M_{h,i} (X_i - \bar{X})^2}{M_{\text{tot}}}} \quad (8)$$

$$R_{e,\perp} = \sqrt{\frac{\sum_i M_{h,i} [(Y_i - \bar{Y})^2 + (Z_i - \bar{Z})^2]}{M_{\text{tot}}}} \quad (9)$$

$$\bar{\mu} = \frac{\sum_i M_{h,i} \mu_i}{M_{\text{tot}}}, \quad \mu = X, Y, Z \quad (10)$$

for each identified proto-cluster, where $M_{h,i}$ is the mass and (X_i, Y_i, Z_i) is the location of the i -th halo in the candidate proto-cluster, $M_{\text{tot}} = \sum_i M_{h,i}$ is the sum of the halo mass in the proto-cluster, and $(\bar{X}, \bar{Y}, \bar{Z})$ is the mass-weighted center. Note that we have assumed that X is in the line-of-sight direction. We only keep member halos that satisfy

$$|X_i - \bar{X}| < R_{e,\parallel} \quad (11)$$

$$\sqrt{(Y_i - \bar{Y})^2 + (Z_i - \bar{Z})^2} < R_{e,\perp}. \quad (12)$$

The black dashed histograms in Fig. 6 show the corresponding distributions. As one can see, the long tail in the low mass end of the distribution is significantly suppressed. All these demonstrate that the use of the proto-clusters identified can effectively improve the link between high- z halos and their descendants at $z = 0$.

4.2 Linking high redshift galaxies to their descendants

Proto-clusters also provide a statistical link between galaxies at high- z and those in the local Universe, thereby allowing us to study the time evolution of the galaxy population. Here we use all galaxies, produced by the empirical model (see § 2.1), with $M_* \geq 10^{10} h^{-1} M_{\odot}$ in halos with $M_h \geq 10^{12} h^{-1} M_{\odot}$ at $z = 1$ and $z = 2$, together with their $z = 0$ descendants identified by following their merging trees.

¹ An interloper is a halo that does not belong to the proto-cluster which the halo is assigned to. It may be a member of another proto-cluster if the two proto-clusters are close to each other.

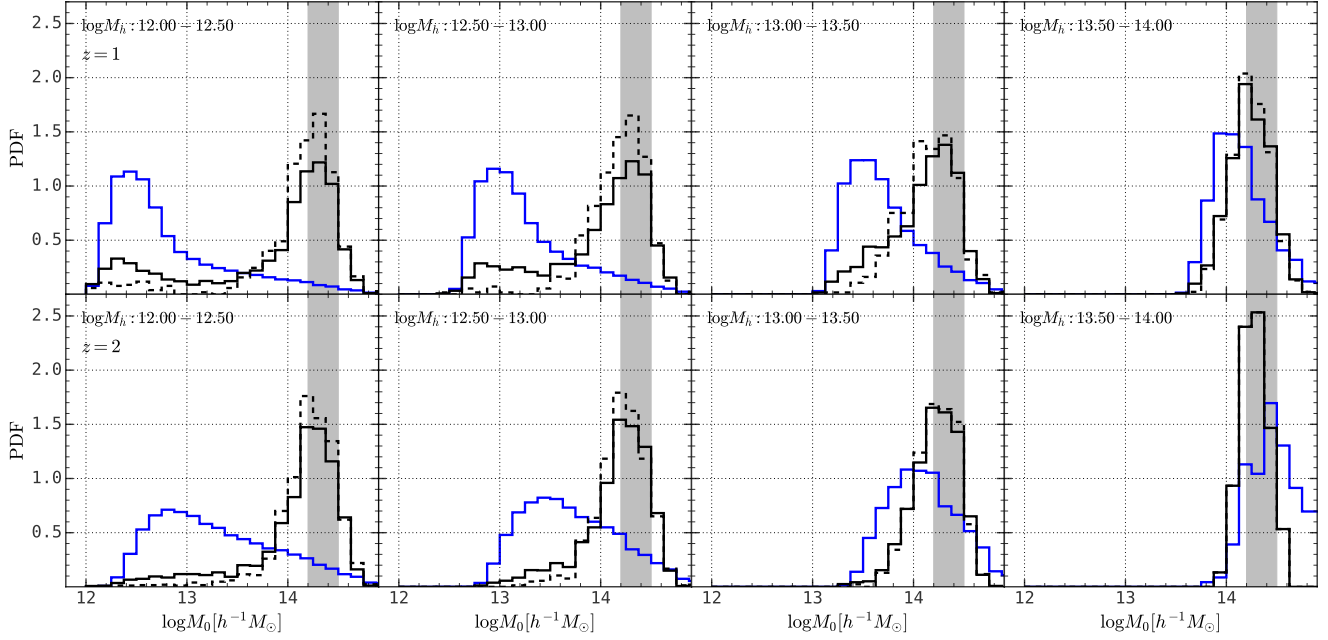


Figure 6. True descendant halo mass distribution for selected dark matter halos at high z . Four *columns* are for dark matter halos selected in different mass bins: $\log(M_h/[h^{-1}M_\odot]) \in [12.0, 12.5]$, $[12.5, 13.0]$, $[13.0, 13.5]$ and $[13.5, 14.0]$. The *blue* histogram shows the true descendant halo mass distribution in each halo mass bin. The *black solid* histogram shows the true descendant halo mass distribution with the additional requirement $14.2 \leq \log(M_{0,e}/[h^{-1}M_\odot]) \leq 14.5$. The *black dashed* histogram shows the true descendant halo mass distribution after eliminating halos in the outskirts of the candidate proto-clusters. The gray region indicates the range of $M_{0,e}$. The *upper panels* are for $z = 1$ and the *lower panels* are for $z = 2$.

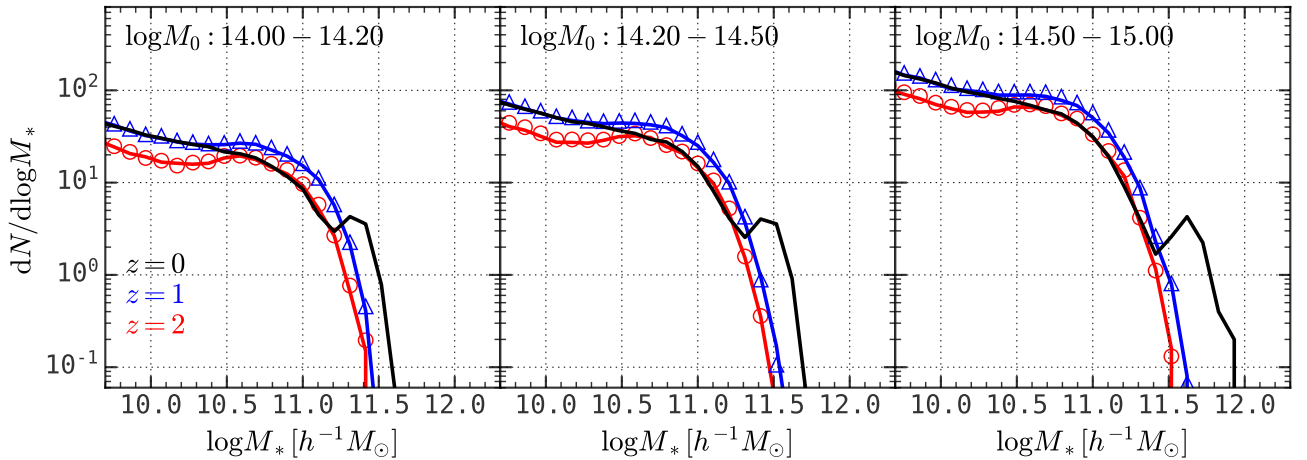


Figure 7. Proto-cluster conditional stellar mass function. The three panels are for different descendant halo mass bins. In each panel, the colored solid lines are results for true proto-clusters and the symbols are for proto-clusters identified with our method. Results are shown for $z = 1$ (*blue*) and $z = 2$ (*red*). For comparison, the black line shows the conditional stellar mass function of galaxies in the $z = 0$ descendant halos.

4.2.1 The conditional stellar mass function of galaxies in proto-clusters

First we examine member galaxies of proto-clusters by studying the conditional stellar mass function of proto-cluster galaxies (hereafter CSMF of PCG), and compare it to the CSMF of cluster galaxies

(hereafter CSMF of CG) at $z = 0$. The CSMF of PCG is defined as

$$\Phi_*(M_*|M_0^l, M_0^u) \equiv \frac{dN(M_*|M_0 \in [M_0^l, M_0^u])}{N_{\text{PC}} d \log M_*} \quad (13)$$

where $N(M_*|M_0 \in [M_0^l, M_0^u])$ is the stellar mass distribution of all the galaxies at high redshift contained in proto-clusters with $M_0^l \leq M_0 \leq M_0^u$, and the normalization factor, N_{PC} , is the number

of proto-clusters in the same M_0 range. Fig. 7 shows the CSMF of PCG measured from the true proto-clusters as solid lines, with blue for $z = 1$ and red for $z = 2$. The result obtained from the identified proto-clusters, shown in circles, matches that for the true proto-clusters very well, indicating that the identified proto-clusters can be used to represent the galaxy population in the true proto-clusters reliably. The black curves are the CSMFs of CG at $z = 0$. As one can see, the number of galaxies increases between $z = 2$ and $z = 1$ by a factor of about two over the entire stellar mass range. Between $z = 1$ and $z = 0$, the number of galaxies at $M_* < 10^{10.5} h^{-1} M_\odot$ changes little, the number around $M_* = 10^{11} h^{-1} M_\odot$ decreases by a factor of ~ 1.5 , while the number at the massive end increases by a large amount. Note that the peak at the massive end is dominated by central galaxies in $z = 0$ clusters. Such a feature is absent at higher z , indicating that the build-up of the mass of central galaxies by accretion happens mostly below $z = 1$. Clearly, such conditional stellar mass functions carry important information about the evolution of the galaxy population in clusters of galaxies.

4.2.2 Descendant mass distribution

We first examine the descendants of galaxies selected at high z . To this end, we select all galaxies at a given z in stellar mass bins and examine their descendant galaxies at $z = 0$. In Fig. 8, the dashed contours show the distribution of the descendants in the stellar mass ($M_{*,0}$) versus halo mass (M_0) space. Results are shown for galaxies selected at $z = 1$ and $z = 2$ in three bins of M_* : $\log(M_*/[h^{-1} M_\odot]) \in [10.0, 10.6]$, $[10.6, 11.2]$, $[11.2, \infty]$, corresponding to the three columns of the figure. As one can see, if restriction is only imposed on the stellar mass of high- z galaxies, the descendants mostly reside in low-mass halos, particularly for the low M_* bins.

Since galaxy properties in the local universe are observed to depend strongly on their host halo mass (e.g. Weinmann et al. 2006; Wang et al. 2018), it is interesting to focus on galaxies that end up in halos/clusters of a given mass in the local Universe. We thus present the joint distribution in $(M_{*,0}, M_0)$ for galaxies of given M_* that are contained in proto-clusters of given estimated descendant halo mass, $M_{0,e}$. In Fig. 8, the black points show the distribution of $(M_*, M_{0,e})$ for the high- z galaxies, while the solid contours show the descendant distributions in $(M_{*,0}, M_0)$. Results are only shown for $14.2 \leq \log(M_{0,e}/[h^{-1} M_\odot]) \leq 14.5$; results for other $M_{0,e}$ bins are similar and omitted for brevity. Here one can see that the descendant halo mass distribution matches the input range of $M_{0,e}$. This is expected, because the proto-clusters identified with our method correspond to their descendants accurately.

It is interesting to note that, for low- M_* galaxies at $z = 1$, the distribution of their descendant galaxies shows two peaks and a middle valley, while for $z = 2$, the distribution shows three peaks. We believe that these three populations correspond to three evolution tracks. Galaxies in the low mass peak have been quenched and experienced no major mass acquisitions since $z = 1$ or $z = 2$, so that their stellar mass does not grow much. The middle valley at $z = 1$ or the middle peak at $z = 2$ corresponds to central galaxies of low mass halos, in which the stellar mass grows steadily through star formation before they are accreted into the cluster at later time. Finally, the high mass peaks correspond to high- z galaxies that have merged with massive galaxies by $z = 0$, so that their descendant stellar mass is much larger than their stellar mass at high z . The low-mass component is more prominent at $z = 1$ compared with $z = 2$, because the time interval available for star formation and merger is shorter. For the most massive galaxies, the increase of the stellar mass in the

descendants is modest, about a factor of 1.5 to 2. We note that the results here are based on the empirical model (Lu et al. 2014, 2015; Chen et al. 2019). However, the evolution tracks of cluster galaxies discussed above are expected to be valid in the general paradigm of galaxy formation.

4.2.3 Abundance matching

Next, we examine the progenitors of the galaxies in $z = 0$ clusters. Because of merger, each galaxy at $z = 0$ may correspond to more than one galaxy at high z . Thus, we consider only the most massive progenitors. Fig. 9 shows the stellar mass distribution of the most massive progenitors at $z = 1$ (upper panels) and $z = 2$ (lower panels) for $z = 0$ galaxies with different stellar masses, $M_{*,0}$. For illustration, results are shown for halos/clusters with $M_0 \geq 10^{14} h^{-1} M_\odot$. The gray filled histogram shows the distribution of true progenitor galaxies identified with the galaxy merging trees in the empirical model. Our goal is to recover this distribution from the proto-clusters identified with our method by linking cluster galaxies with the most massive progenitors at high z .

As a first attempt, we use a simple abundance matching scheme, assuming that more massive galaxies at $z = 0$ have more massive progenitors at high z (van Dokkum et al. 2010; Behroozi et al. 2013). We first separate galaxies at a given high z according to the estimated descendant halo mass, $M_{0,e}$. For each galaxy at $z = 0$, we then match it with a high- z galaxy that has the same stellar mass rank in the same $M_{0,e}$ bin. The blue histograms in Fig. 9 show the results of the progenitor stellar mass distribution obtained from this scheme. For high $M_{*,0}$, the scheme reproduces the distribution quite well. For low $M_{*,0}$, however, the distribution is biased towards the massive end relative to the true distribution. This bias is caused by galaxy merging. As shown in Fig. 8, many high- z galaxies with intermediate stellar masses have merged into massive descendants by $z = 0$. A fraction of these galaxies should not be used in the abundance matching, as they are not the most massive progenitors of any galaxies at $z = 0$.

To deal with the problem caused by galaxy merging in the abundance matching, we need to exclude, in the abundance matching scheme, galaxies that are not the most massive progenitors of any galaxies at $z = 0$. In real applications, this can be done only in a statistical sense, as one cannot establish the merger trees for individual galaxies in observation. Statistically, we can estimate the fraction of the most massive progenitors among all progenitors of given properties: $F_{\text{mmp}}(z) = N_{\text{mmp}}(z)/N_{\text{all}}(z)$, where $N_{\text{mmp}}(z)$ is the number of the most massive progenitors at z for galaxies at $z = 0$, and $N_{\text{all}}(z)$ is the number of all galaxies. This fraction can be estimated from our empirical model or from numerical simulations, and the hope is that it can be presented in a way such that it does not depend on galaxy formation model strongly (see Appendix C for a test). To achieve this, we first divide galaxies at a given high z into bins of their host halo masses, M_h . Each galaxy is assigned a rank according to its stellar mass rank in its halo, with the first rank corresponding to the most massive galaxy and so on. F_{mmp} is estimated in each (M_h, rank) bin and presented in Fig. 10 for $z = 1$ (left panel) and $z = 2$ (right panel). Once F_{mmp} is known, we can randomly select galaxies at high z as the most massive progenitor of a galaxy at $z = 0$ with a probability F_{mmp} . The abundance matching scheme can then be used between $z = 0$ galaxies and the galaxies in the random sample of the most massive progenitors to establish, statistically, connections between $z = 0$ cluster galaxies and their progenitors. The red histograms in Fig. 9 show the mass distributions of the most massive progenitors matched in this way. These distributions match the true distribution (the shaded histograms) well, indicating that our method provides

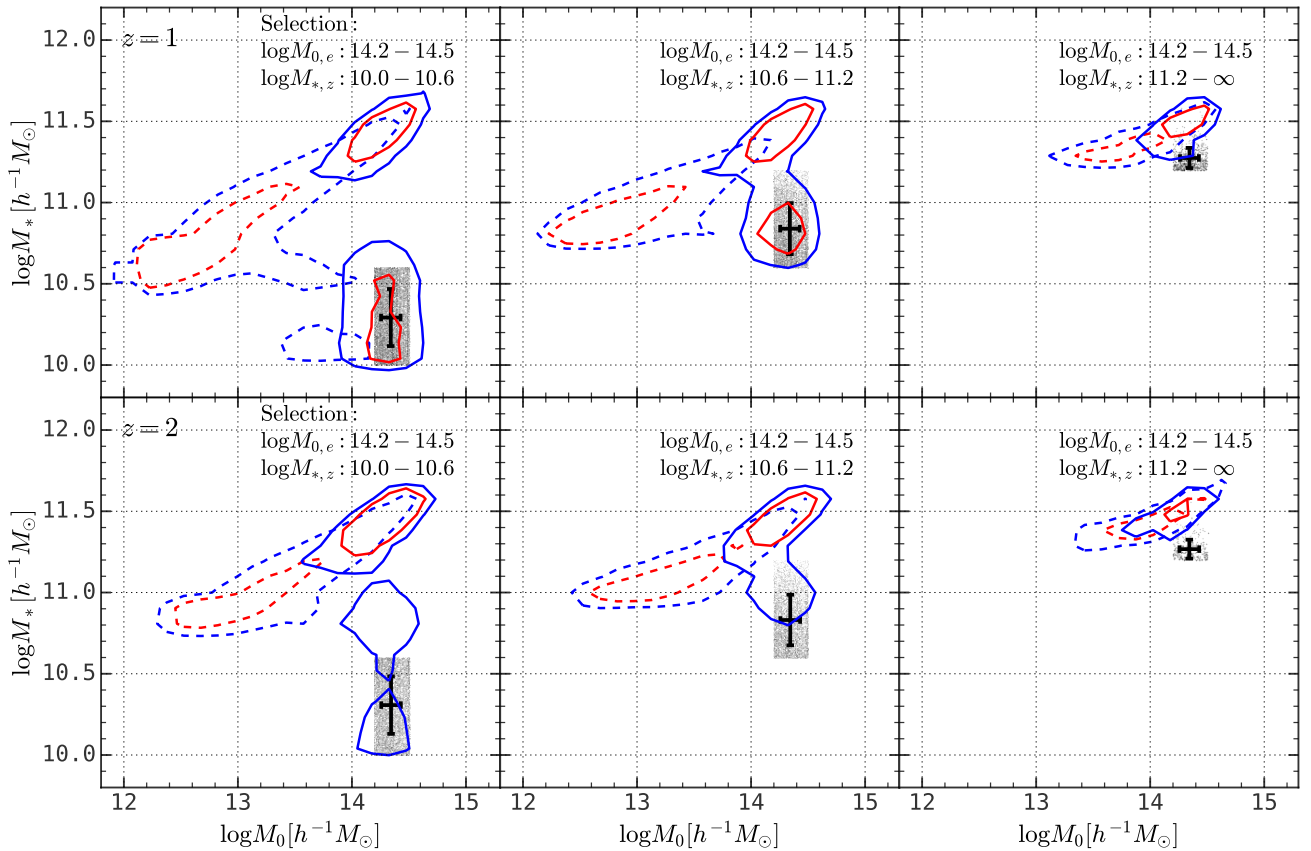


Figure 8. Joint distribution in descendant halo mass and descendant stellar mass. The three *columns* are for galaxies in different stellar mass bins: $[10.0, 10.6]$, $[10.6, 11.2]$, and $[11.2, \infty]$ selected at high z . The *dashed* and *solid* contours both show the joint distribution in the true descendant halo mass (M_0) and descendant stellar mass ($M_{*,0}$) distribution, with the dashed ones for galaxies selected only with stellar mass (M_*), and the solid ones for galaxies selected with both the stellar mass (M_*) and the additional requirement that $14.2 \leq \log(M_{0,e}/[h^{-1}M_\odot]) \leq 14.5$, indicated by the black points. The error bar shows the mean and standard deviation of the black points. The *blue* and *red* contours enclose 80% and 50% of the galaxies, respectively. The *upper* panels are for $z = 1$ and the *lower* panels are for $z = 2$.

a statistically reliable way to link galaxies to their progenitors. As shown in Appendix B, our method also performs better than those used in the literature to link the brightest central galaxies (BCGs) to their progenitors. Note that different realizations of F_{mmp} lead to different samples of the most massive progenitors. The variance among these samples provides a useful measure of the uncertainty in the abundance matching scheme. Finally, we note that the distribution of F_{mmp} shown in Fig. 10 is bimodal. Galaxies of Rank = 1 are the most massive centrals in their halos, and are expected to experience different mergers than satellites in the subsequent evolution.

5 SUMMARY

In this paper, we develop a method to identify proto-clusters from halos/groups identified in galaxy surveys at high z . We demonstrate how the information provided by groups and proto-clusters can be used to establish the connections of cluster galaxies in the present-day universe to their high- z progenitors. Our proto-cluster finder is based on an extension of the traditional FoF algorithm applied to dark matter halos represented by galaxy groups/clusters. Compared with previous methods of proto-cluster identification, our method does not depend

on details of how galaxies form in dark matter halos. Our main results can be summarized as follows.

- (i) Using samples of halos and galaxies in simulations, we find that our proto-cluster finder can identify $\geq 85\%$ of the true proto-clusters with purity $\geq 95\%$. The standard deviation in the descendant halo mass estimate is smaller than 0.25 dex.
- (ii) For the assignments of member halos to proto-clusters, our test shows that $\sim 70\%$ of the candidate proto-clusters have both completeness and purity $\geq 80\%$ in halo memberships.
- (iii) We show that the proto-clusters identified by our method provide important information to link halos and galaxies across different redshifts. With the help of proto-clusters, one can effectively select halos and galaxies at high z that are progenitors of clusters and cluster galaxies at the present day. This can help us understand the evolution history for galaxies in local clusters.
- (iv) We find that the mass function of member halos and the stellar mass function of member galaxies in true proto-clusters are well reproduced by the proto-clusters selected with our method.
- (v) The comparison of the galaxy population in proto-clusters with that in present-day clusters carries important information about the evolution of cluster galaxies. We find that relatively low-mass

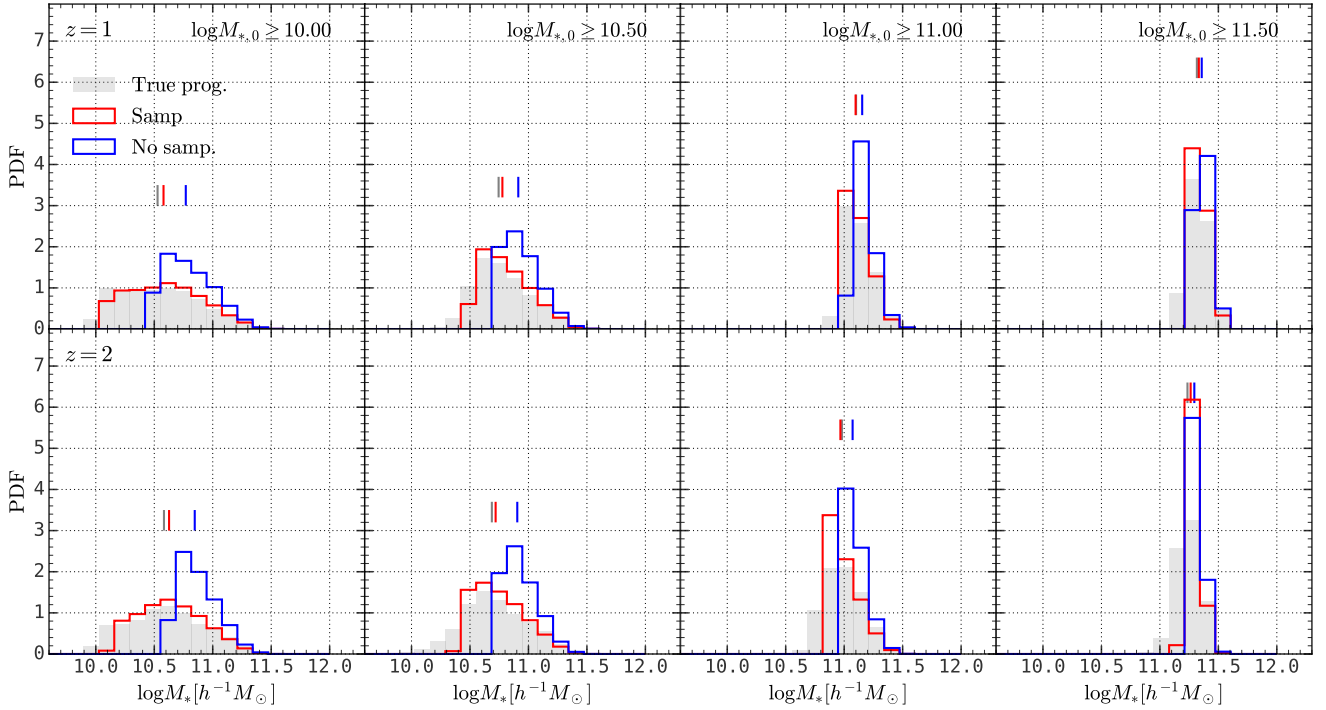


Figure 9. Stellar mass distribution of the most massive progenitor galaxies at $z = 1$ (upper) and $z = 2$ (lower) for galaxies selected at $z = 0$ with different stellar mass cuts (different columns). The gray histograms show the true distribution extracted from the galaxy merger tree, while the red and blue are the results using rank matching method with or without the sampling process, respectively (See text). The short colored bars in each panel indicate the medians of the histograms of the corresponding colors.

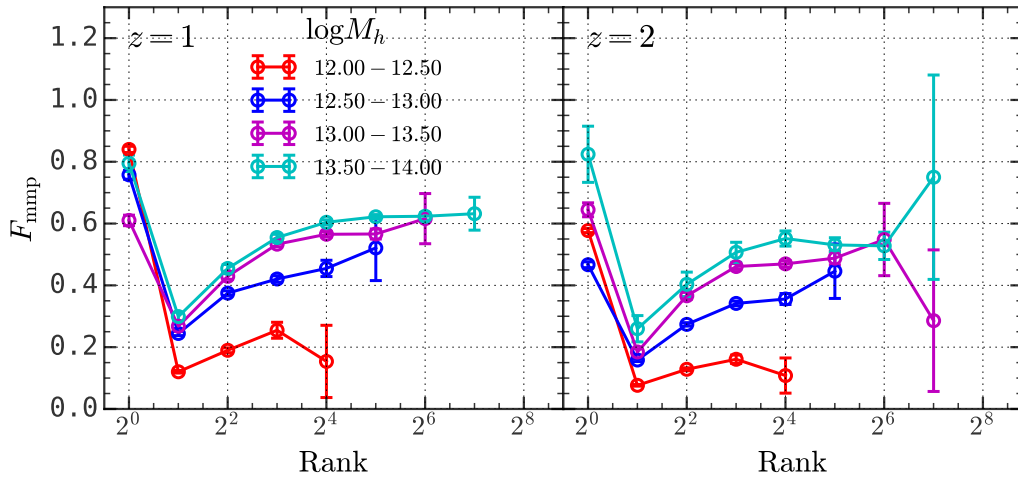


Figure 10. Fraction of the most massive progenitors, F_{mmp} , as a function of stellar mass rank in their host halo for galaxies at $z = 1$ (left) and $z = 2$ (right). Different colors are for different halo mass bins.

galaxies in proto-clusters in general can be divided into three different populations: galaxies whose stellar mass changed little during the redshift range in question; galaxies that have increased their stellar mass significantly by star formation before quenched by the cluster environment; galaxies that have merged into more massive galaxies.

Massive galaxies typically increase their stellar mass by accreting lower-mass galaxies.

(vi) We develop an abundance matching method to connect galaxies in proto-clusters with their descendants in present-day clusters, taking into account the bias produced by mergers of galaxies. We find that the probability for a high- z galaxy in a proto-cluster to be the

most massive progenitor of a cluster galaxy at the present day can be calibrated reliably in a way without depending on the details of the galaxy formation process. Our test shows that this probability can be used to successfully recover the progenitor stellar mass distribution for galaxies in local clusters.

Our method can be applied straightforwardly to real surveys of high- z galaxies, such as zCOSMOS (Lilly et al. 2009), PFS (Takada et al. 2014), and any other surveys from which galaxy groups/clusters can be identified reliably to represent the dark matter halo population. We have tested the impact of a number of general uncertainties, such as redshift-space distortion, incompleteness of groups/clusters, and uncertainties in halo mass estimates, and found that our method works reliably under the influences of these uncertainties. In real applications, we may still need to test the method using realistic mock catalogs to quantify the impact of selection effects in a specific survey, but this is straightforward to do. With the advent of large surveys of high- z galaxies, we expect that our method will provide a new avenue to investigate the formation and evolution of clusters of galaxies as well as the evolution of their galaxy populations.

ACKNOWLEDGEMENTS

This work is supported by the National Key R&D Program of China (grant No. 2018YFA0404502, 2018YFA0404503), and the National Science Foundation of China (grant Nos. 11821303, 11973030, 11673015, 11733004, 11761131004, 11761141012). We acknowledge Dandan Xu, Yuning Zhang and Jingjing Shi for accessing the TNG simulation data. Kai Wang and Yangyao Chen gratefully acknowledge the financial support from China Scholarship Council.

DATA AVAILABILITY

The data products of this article will be available on requests to the corresponding author. The computation was supported by the HPC toolkit **HIPP** at <https://github.com/ChenYangyao/hipp>.

REFERENCES

Behroozi P. S., Marchesini D., Wechsler R. H., Muzzin A., Papovich C., Stefanon M., 2013, *The Astrophysical Journal*, 777, L10
 Cai Z., et al., 2016, *The Astrophysical Journal*, 833, 135
 Cai Z., et al., 2017, *The Astrophysical Journal*, 839, 131
 Chen Y., Mo H. J., Li C., Wang H., Yang X., Zhou S., Zhang Y., 2019, *The Astrophysical Journal*, 872, 180
 Chiang Y.-K., Overzier R., Gebhardt K., 2013, *The Astrophysical Journal*, 779, 127
 Chiang Y.-K., Overzier R., Gebhardt K., 2014, *The Astrophysical Journal*, 782, L3
 Chiang Y.-K., et al., 2015, *The Astrophysical Journal*, 808, 37
 Cimatti A., Nipoti C., Cassata P., 2012, *Monthly Notices of the Royal Astronomical Society: Letters*, 422, L62
 Clauwens B., Franx M., Schaye J., 2016, *Monthly Notices of the Royal Astronomical Society: Letters*, 463, L1
 Cooke K. C., Kartaltepe J. S., Tyler K. D., Darvish B., Casey C. M., Fèvre O. L., Salvato M., Scoville N., 2019, *The Astrophysical Journal*, 881, 150
 Davis M., Efstathiou G., Frenk C. S., White S. D. M., 1985, *The Astrophysical Journal*, 292, 371
 DeMaio T., et al., 2020, *Monthly Notices of the Royal Astronomical Society*, 491, 3751
 Diener C., et al., 2013, *The Astrophysical Journal*, 765, 109

Dunkley J., et al., 2009, *The Astrophysical Journal Supplement Series*, 180, 306
 Eke V. R., et al., 2004, *Monthly Notices of the Royal Astronomical Society*, 348, 866
 Fakhouri O., Ma C.-P., Boylan-Kolchin M., 2010, *Monthly Notices of the Royal Astronomical Society*, 406, 2267
 Franck J. R., McGaugh S. S., 2016, *The Astrophysical Journal*, 817, 158
 Hearin A. P., et al., 2017, *The Astrophysical Journal*, 154, 190
 Hill A. R., et al., 2017, *The Astrophysical Journal*, 837, 147
 Jackson J. C., 1972, *Monthly Notices of the Royal Astronomical Society*, 156, 1P
 Kaiser N., 1987, *Monthly Notices of the Royal Astronomical Society*, 227, 1
 Kipper R., Tamm A., Tempel E., de Propris R., Ganeshiah Veena P., 2021, *Astronomy and Astrophysics*, 647, A32
 Knobel C., et al., 2009, *The Astrophysical Journal*, 697, 1842
 Lee K.-G., et al., 2016, *The Astrophysical Journal*, 817, 1
 Lidman C., et al., 2012, *Monthly Notices of the Royal Astronomical Society*, 427, 550
 Lilly S. J., et al., 2009, *The Astrophysical Journal Supplement Series*, 184, 218
 Lin Y.-T., Brodwin M., Gonzalez A. H., Bode P., Eisenhardt P. R. M., Stanford S. A., Vikhlinin A., 2013, *The Astrophysical Journal*, 771, 61
 Looser T. J., Lilly S. J., Sin L. P. T., Henriques B. M. B., Maiolino R., Cirasuolo M., 2021, arXiv:2104.07664 [astro-ph]
 Lovell C. C., Thomas P. A., Wilkins S. M., 2018, *Monthly Notices of the Royal Astronomical Society*, 474, 4612
 Lu Z., Mo H. J., Lu Y., Katz N., Weinberg M. D., van den Bosch F. C., Yang X., 2014, *Monthly Notices of the Royal Astronomical Society*, 439, 1294
 Lu Z., Mo H. J., Lu Y., Katz N., Weinberg M. D., van den Bosch F. C., Yang X., 2015, *Monthly Notices of the Royal Astronomical Society*, 450, 1604
 Martinache C., et al., 2018, *Astronomy & Astrophysics*, 620, A198
 Mendel J. T., et al., 2020, *The Astrophysical Journal*, 899, 87
 Nelson D., et al., 2019, *Computational Astrophysics and Cosmology*, 6, 2
 Overzier R. A., 2016, *The Astronomy and Astrophysics Review*, 24, 14
 Pillepich A., et al., 2018, *Monthly Notices of the Royal Astronomical Society*, 475, 648
 Springel V., White S. D. M., Tormen G., Kauffmann G., 2001, *Monthly Notices of the Royal Astronomical Society*, 328, 726
 Springel V., et al., 2005, *Nature*, 435, 629
 Steidel C. C., Adelberger K. L., Dickinson M., Giavalisco M., Pettini M., Kellogg M., 1998, *The Astrophysical Journal*, 492, 428
 Steidel C. C., Adelberger K. L., Shapley A. E., Erb D. K., Reddy N. A., Pettini M., 2005, *The Astrophysical Journal*, 626, 44
 Takada M., et al., 2014, *Publications of the Astronomical Society of Japan*, 66, R1
 Torrey P., et al., 2015, *Monthly Notices of the Royal Astronomical Society*, 454, 2770
 Torrey P., Wellons S., Ma C.-P., Hopkins P. F., Vogelsberger M., 2017, *Monthly Notices of the Royal Astronomical Society*, 467, 4872
 Toshikawa J., et al., 2016, *The Astrophysical Journal*, 826, 114
 Wang H., et al., 2016, *The Astrophysical Journal*, 831, 164
 Wang H., et al., 2018, *The Astrophysical Journal*, 852, 31
 Wang K., Mo H. J., Li C., Meng J., Chen Y., 2020, *Monthly Notices of the Royal Astronomical Society*, 499, 89
 Weinmann S. M., Van Den Bosch F. C., Yang X., Mo H. J., 2006, *Monthly Notices of the Royal Astronomical Society*, 366, 2
 Yang X., Mo H. J., van den Bosch F. C., Jing Y. P., 2005, *Monthly Notices of the Royal Astronomical Society*, 356, 1293
 Yang X., Mo H. J., van den Bosch F. C., Pasquali A., Li C., Barden M., 2007, *The Astrophysical Journal*, 671, 153
 Zhao D., Conselice C. J., Aragón-Salamanca A., Almaini O., Hartley W. G., Lani C., Mortlock A., Old L., 2017, *Monthly Notices of the Royal Astronomical Society*, 464, 1393
 van Dokkum P. G., et al., 2010, *The Astrophysical Journal*, 709, 1018

APPENDIX A: UNCERTAINTIES INTRODUCED BY THE GROUP FINDER

As shown in Wang et al. (2020), a well-designed group finder applied to high- z redshift surveys such as the PFS can achieve a completeness of $\geq 90\%$ with a halo mass uncertainty of about 0.2 dex for galaxy groups/clusters above $10^{12}h^{-1}M_{\odot}$. These uncertainties will also affect the performance of the proto-cluster identification, as our method is based on halos. Here we employ two additional mocks to mimic uncertainties introduced by the galaxy group finding process. Thus we make comparisons between the following three mocks:

- **Mock-1:** The same as the mock used in the main part of the paper.

- **Mock-2:** Add the following uncertainty to halo mass:

$$\log M_h \leftarrow \log M_h + N(0, 0.2) \quad (\text{A1})$$

where $N(0, 0.2)$ is a random number generated from a Gaussian distribution with mean $\mu = 0$ and dispersion $\sigma = 0.2$.

- **Mock-3:** Add the same halo mass uncertainty as in **Mock-2**. In addition we randomly drop 10% of the halos to mimic the incompleteness produced by the group finding process.

Fig. A1 shows the result of group-level performance at $z = 2$. We can see that the completeness and purity for $\epsilon_M = \infty$ are nearly unchanged, while the performance decreases for $\epsilon_M = 0.4$, which is caused by the error in the descendant halo mass calibration. Here we only show the result of $z = 2$ for brevity since the result of $z = 1$ has a similar trend. For the member level performance, the results is nearly the same as those shown in Fig. 4, so we also omit it. This result also verifies that the decreasing of the group-level performance is caused by the descendant halo mass calibration, instead of the member halo assignment. We also present the standard deviation for the descendant halo mass calibration in Fig. A2. One can see that the error is increased by both the halo mass uncertainty and halo incompleteness. The conditional halo mass functions obtained from all the three mocks are shown in Fig. 5. As one can see, the results for **Mock-2** and **Mock-3** are very similar to that for **Mock-1**, except at the massive end where the halo mass functions are overestimated because of the larger uncertainty in the halo mass.

APPENDIX B: THE BRIGHTEST CENTRAL GALAXIES OF CLUSTERS AND THEIR PROGENITORS

Some previous investigations have attempted to link the brightest cluster galaxies across different redshifts by integrating the mass accretion rate to get the descendant halo mass at $z = 0$ using the formula in Fakhouri et al. (2010) (See Lidman et al. 2012; Cooke et al. 2019; DeMaio et al. 2020; Lin et al. 2013). Here we compare our method with this, and we denote the method of Lidman et al. (2012) as the BCG method and ours the PC method for convenience. For central galaxies at $z = 0$ with halo mass in a mass bin, the BCG method identifies all the halos at a given redshift (in our case, $z = 1$ or $z = 2$) whose descendant mass at $z = 0$ is in the same mass bin, while the PC method selects all central galaxies of the most massive halos (MMH) in candidate proto-clusters whose estimated descendant halo mass is in a given mass bin. In each descendant halo mass bin, we define the **completeness** as the fraction of centrals at $z = 0$ whose progenitors are selected at $z = 1$ or 2, and the **purity** as the fraction of the selected galaxies at $z = 1$ or 2 which are the true progenitors of the central galaxies in the descendant halo mass bin in question. The comparison is presented in Fig. B1, with black lines showing results for the BCG method and the blue lines for the PC method. At $z = 1$,

the BCG method performs slightly better in purity at the massive end, but it is at the cost of a much worse performance in completeness. At $z = 2$, the PC method performs better, especially in purity. Note that the absolute values of the completeness and purity depend on the choice of the mass bin size, because the mass bin size here is equivalent to the tolerance of descendant halo mass error.

APPENDIX C: TEST USING ILLUSTRIS-TNG

As a test, we apply the method in § 4.2.3 to galaxies in Illustris TNG300-1 simulation (Nelson et al. 2019; Pillepich et al. 2018). In Fig. C1, we show the stellar mass distribution of the most massive progenitors for galaxies at $z = 0$ with $M_0 \geq 10^{14}h^{-1}M_{\odot}$. The gray histogram shows the true distribution, where the most massive progenitors are identified from the galaxy merger tree in TNG300-1. One can see that the true distribution is distinct from the results shown in Fig. 9 due to the difference in the galaxy formation models. To recover this distribution, we first perform the same abundance matching as in § 4.2.3, and the results are shown as the blue histograms. The predicted distributions are biased towards the high mass end due to mergers of galaxies. To deal with this problem, we again randomly select galaxies in TNG300-1 at $z = 1$ and $z = 2$ according to the F_{mmp} shown in Fig. 10. We emphasize that the F_{mmp} model is adopted from the empirical model instead of the TNG300-1 simulation. We then apply the abundance matching to find the most massive progenitors for galaxies at $z = 0$, and the results are shown as the red histograms. The bias relative to the true distribution is now much reduced, indicating that F_{mmp} is independent of the details of the galaxy formation model.

This paper has been typeset from a \LaTeX file prepared by the author.

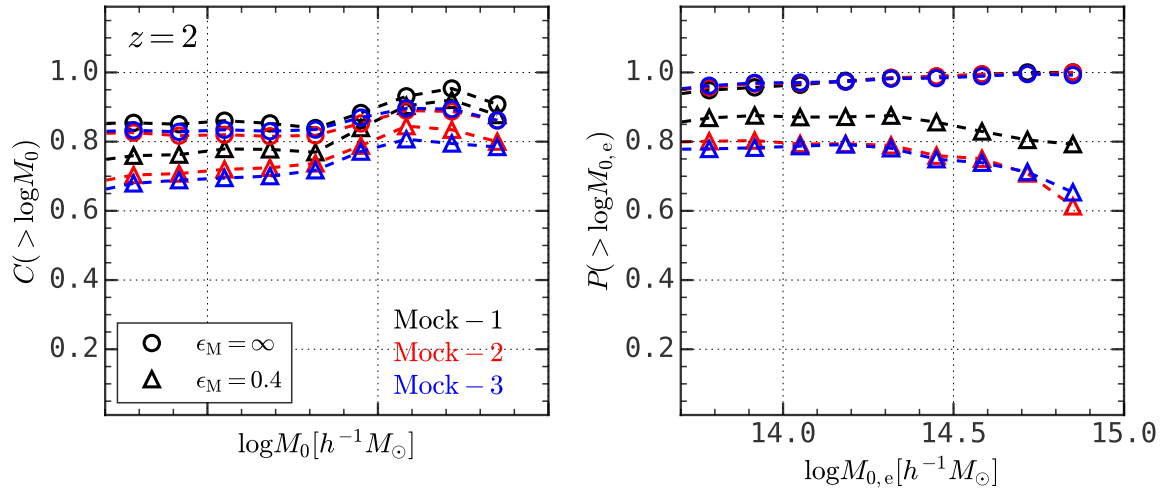


Figure A1. Same as Fig. 2 at $z = 2$. The black lines are for Mock-1, the red lines are for Mock-2 and the blue lines are for Mock-3.

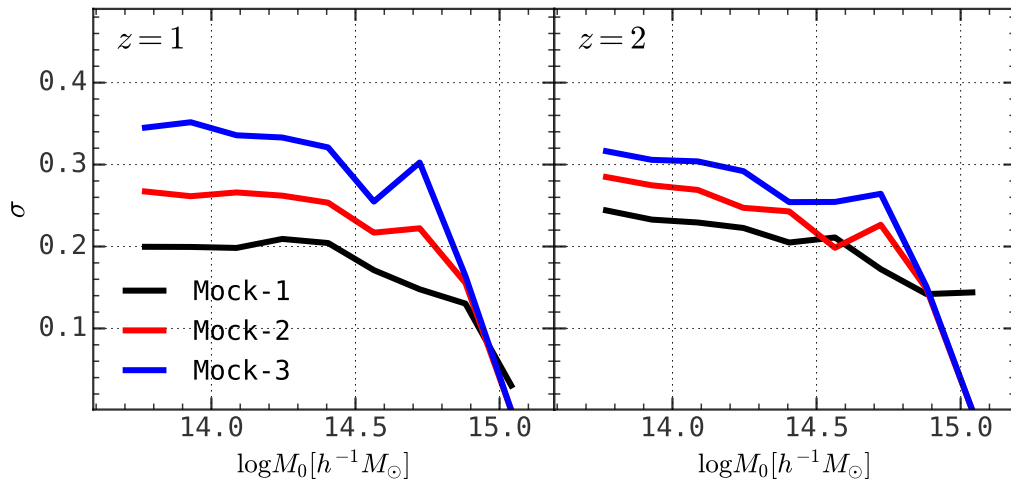


Figure A2. Same as the lower panels in Fig. 3. The black lines are for Mock-1, the red lines are for Mock-2 and the blue lines are for Mock-3.

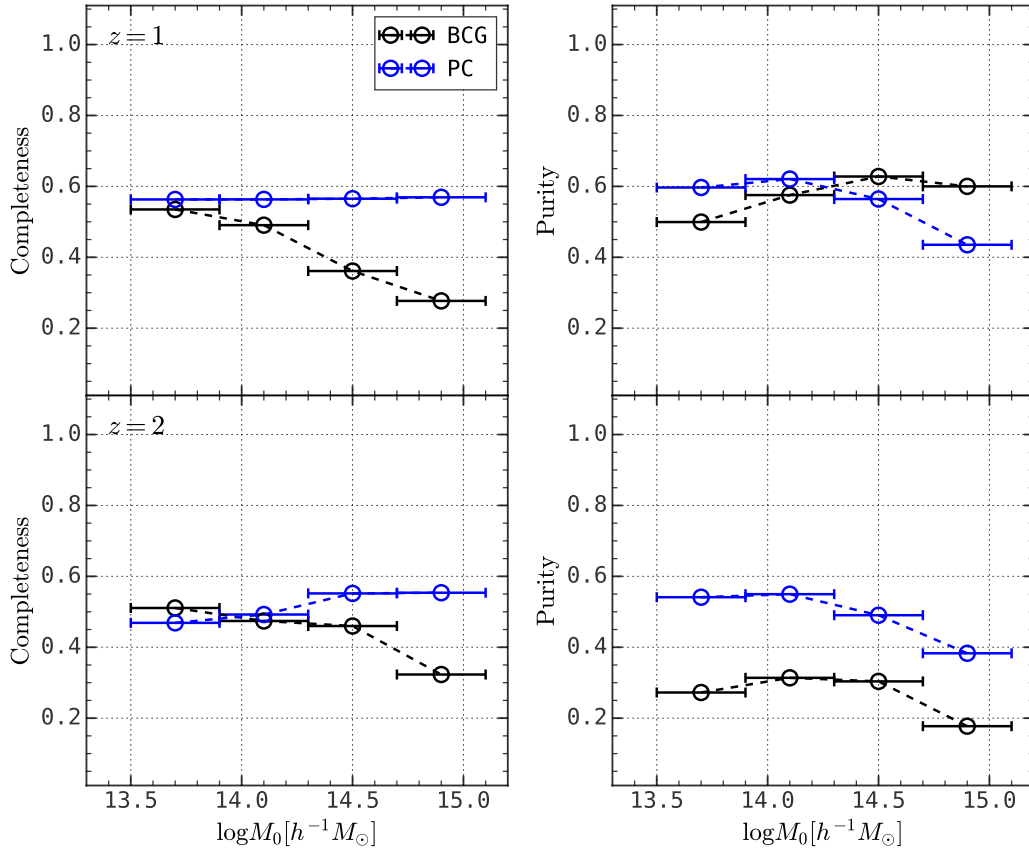


Figure B1. Comparison of the performance in connecting central galaxies at $z=0$ and $z=1$ (2). The black lines are for BCG method and blue lines are for PC method (See text). The upper panels are for $z=1$ and lower panels are for $z=2$.

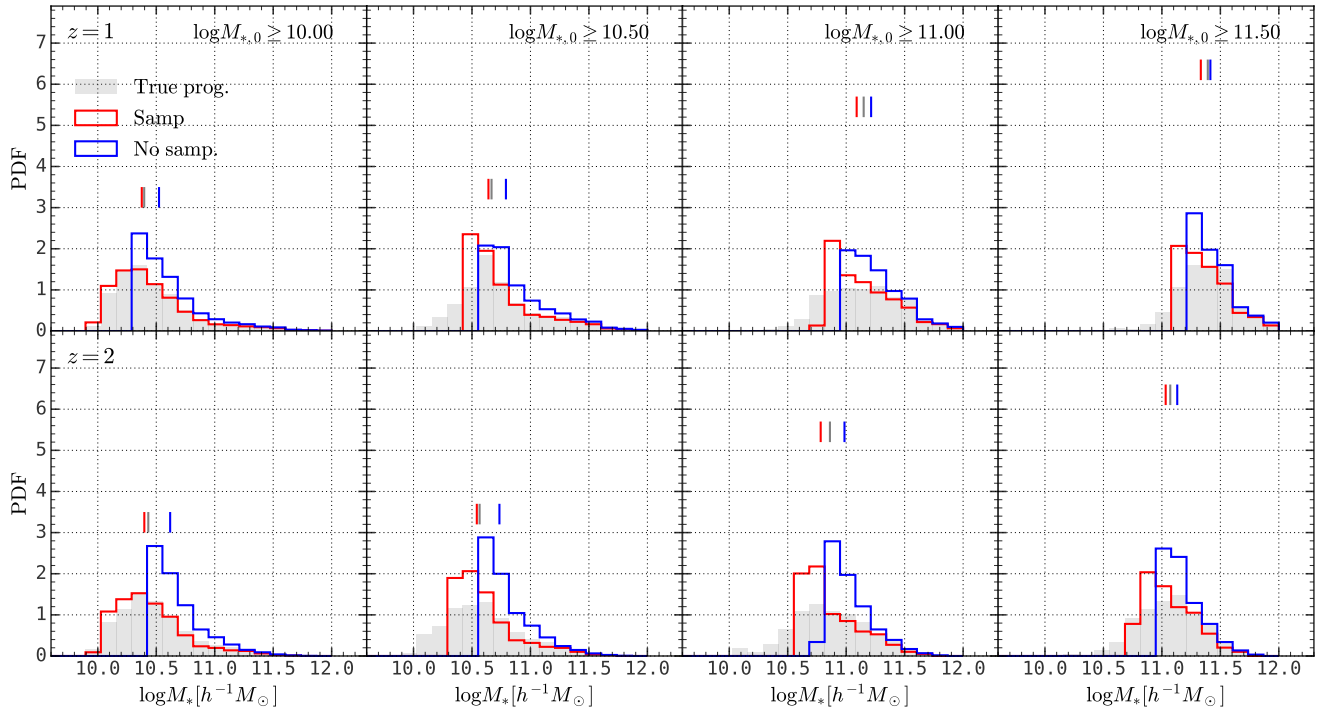


Figure C1. Same as Fig. 9, just for galaxies in Illustris TNG300-1 simulation.